Multi-hole plastic optical fiber force sensor based on femtosecond laser micromachining

Guoyu Tang (汤国玉), Jue Wei (韦 珏), Wei Zhou (周 薇), Ruiqin Fan (范瑞琴), Mingyu Wu (吴明宇), and Xiaofeng Xu (徐晓峰)*

College of Physics, Jilin University, Changchun 130012, China

**Corresponding author: xuxf@jlu.edu.cn*

Received April 8, 2014; accepted June 11, 2014; posted online August 28, 2014

We study the theoretical and experimental effects of hole quantity and inter–inter-hole spacing on insertion loss for using femtosecond laser to make bend-sensitive multi-hole plastic optical fiber (POF), and also analyze the mechanism of bending loss in multi-hole POF. A force sensor based on bending loss of the multi-hole POF is fabricated. The measurement ranges from 0 to 65 N, and the maximum output change exceeds 15.51 dB with good linearity and repeatability, and the sensitivity is 0.24 dB/N.

OCIS codes: 060.2370, 060.2310.

doi: 10.3788/COL201412.090604.

Plastic optical fiber (POF) has the advantages of low cost, pliable and large diameter, etc. The technology and applications of POF have progressed rapidly in recent years. A large number of sensors based on POF have been developed, such as breathing, alcohol, displacement, temperature, and refractive index sensors[1–5]. Optical fiber pressure sensor has the advantages of small volume, high measuring accuracy, and quick response, and has been widely studied. The pressure sensors based on optical fiber include fiber Bragg grating[6,7], taper fiber[8], distributed optical fiber[9], Fabry-Perot interference[10], and so on. Additionally, this could also be achieved by using the bending loss mechanism of the POF[11].

Femtosecond laser micromachining has the advantages of being able to process on a tiny area and having little thermal effects[12,13]. Femtosecond laser micromachining has been reported[14–16]. Multi-hole POF force sensor based on bending loss is fabricated by femtosecond laser micromachining. The measurement ranges from 0 to 65 N, and the maximum output changes exceed 15.51 dB with good linearity.

The schematic diagram of multi-hole POF is shown in Fig. 1. The refractive indices of the core and the cladding are 1.491 and 1.417, respectively. There are many modes in multimode POF, that is, many light rays with different incident angles propagate in the core. For those light rays, total reflection occurs at the core–cladding interface. However, when the light rays arrive at the hole–core interface, because there is air in hole and the refractive index of air is approximately 1—which is lower than that of the fiber core—the micro-hole will behave as a negative lens and some light rays will deflect and enter into the cladding and will be lost. The remaining light will continue to propagate along the fiber core. Based on Snell's law, the formula for intensity reflectivity is

$$R = \frac{1}{2}\left[\left|\frac{\tan(i_1 - i_2)}{\tan(i_1 + i_2)}\right|^2 + \left|\frac{\sin(i_2 - i_1)}{\sin(i_2 + i_1)}\right|^2\right], \tag{1}$$

$$\frac{n_1}{n_2} = \frac{\sin(i_2)}{\sin(i_1)}. \tag{2}$$

The simulation uses step multimode POF. The fiber-core and cladding outer diameters are 0.96 and 1.0 mm, respectively. The refractive indices of core and cladding are 1.491 and 1.417, respectively. Each micro-hole diameter is approximately 150 μm. The yellow lines in Fig. 1 show the reflected light rays. Using MATLAB software, Fig. 2 models the relationship between light intensity reflectivity and the incident angle α at the core–cladding. Thus it is evident that the smaller the incident angle the lower the light intensity reflectivity and the greater the light intensity entering the cladding—which naturally translates into greater loss.

Moreover, because there is a great difference between the refractive indices of the core and the hole, strong reflection will happen at their interface, as shown by the red lines in Fig. 1. The simulation result in Fig. 3 shows the relationship between light intensity reflectivity and incident angle β. Unlike Fig. 2, at the core–hole interface, the smaller the incident angle at the core–hole interface, the lower the intensity, reflectivity, and the loss.

In view of the aforementioned mechanism, every hole will induce some loss. By increasing the number of holes, the total loss will increase.

In addition to the number of holes, inter-hole spacing can also impact the level of insertion loss. In Fig. 4, suppose the emergent ray from hole 1 can penetrate through the latter holes 2 and 3. As the distance

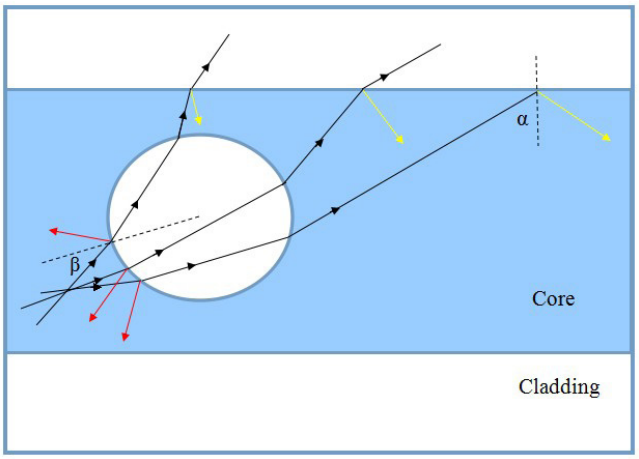

Fig. 1. Diagrammatic sketch of multi-hole POF.

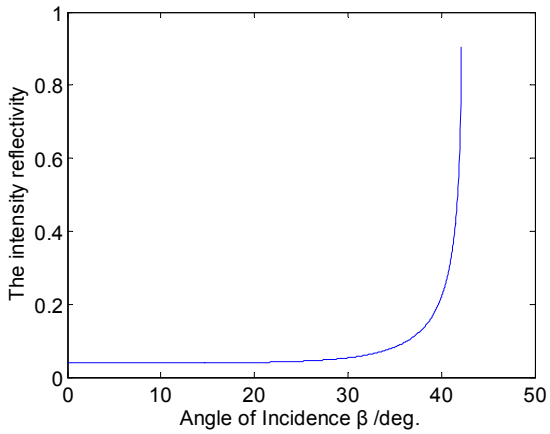

Fig. 3. Relationship between light intensity reflectivity and the incident angle at the interface of fiber core and hole.

between holes increases, the incident angle at the core–hole interface will also increase (i.e., $\theta_1 < \theta_2$, where θ_1 and θ_2 are the incident angles at the core–hole interfaces of holes 2 and 3, respectively). By Snell's law, light ray that passes through the hole will deflect; the angle between the incident ray and the emergent ray is defined as the bending angle. The relationship between the incident angle and the bending angle is shown in Fig. 5. As shown, the bending angle has the same variation trend as the incident angle; therefore it follows that $\theta_4 < \theta_3$ and the light intensity reflectivity at the core–cladding interface will decrease as the incident angle decreases. Therefore, when the number of holes remains the same, loss due to hole-deflection will increase as the holes are spread further apart. However, if the holes are set too far apart, such as the case of holes 1 and 4, the emergent ray from the front hole cannot be deflected by the latter hole. Consequently, as the inter-hole spacing widens, the level of insertion loss will also increase until it peaks at a certain point and then begins to decrease.

Bends in fiber usually cause some transmitted light not to be totally reflected and result in some loss. However, bending loss is not noticeable in multimode POF because large amount of light rays are confined in the fiber core. Figure 6 shows a bent multi-hole POF. If there is no hole in the fiber, light would transmit along the dotted line and the incident angle is still greater

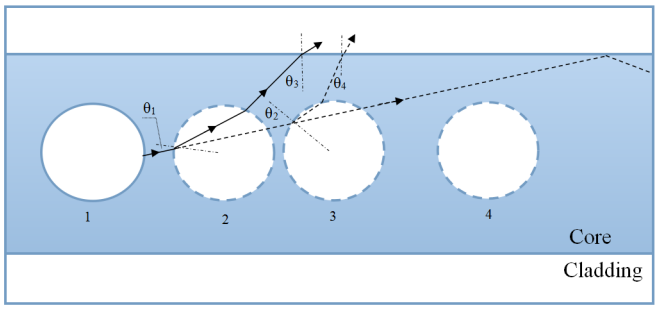

Fig. 4. Schematic diagram of inter-hole spacing.

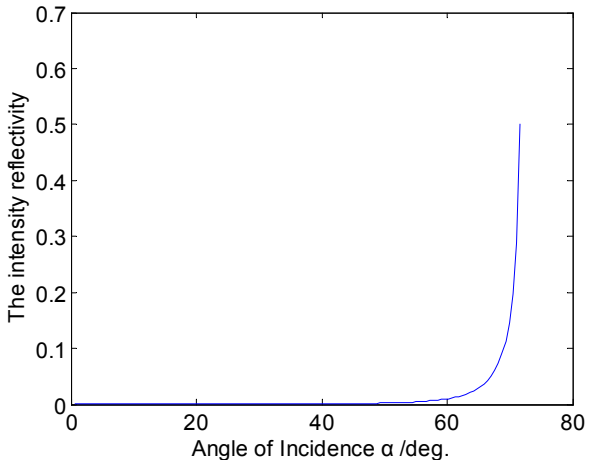

Fig. 2. Relationship between light intensity reflectivity and incident angle at core–cladding interface.

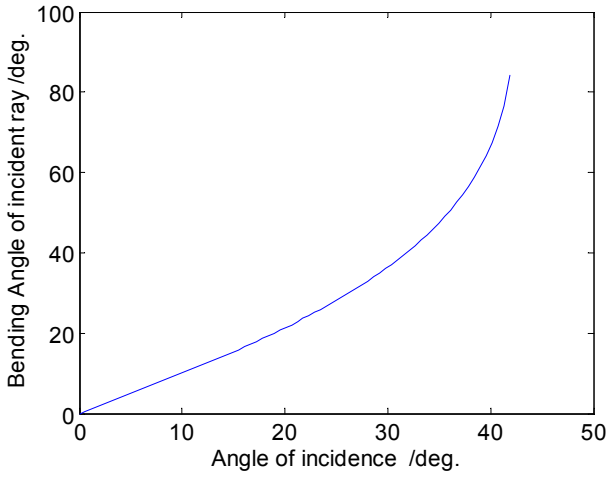

Fig. 5. Relationship between the incident angle and the bending angle.

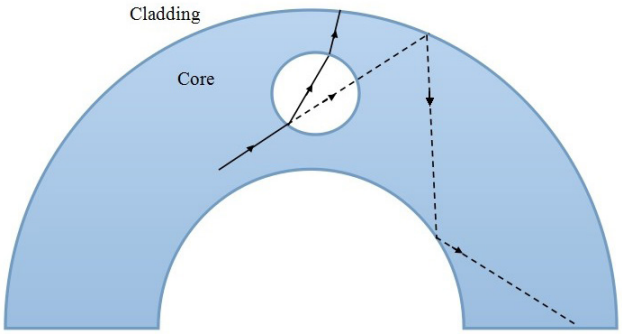

Fig. 6. Bended multi-hole POF.

than the critical angle for total internal reflection. That is to say, even though the POF bends, light can continue to propagate within the core. However, if a hole is introduced and light passes through the hole, the incident angle would be smaller than the critical angle due to deflection and the light ray would be cut off. In such case, bends in the POF will cause more light not to meet the critical angle necessary for total reflection and induce additional loss. Thus, it is evident that multi-hole POF is more sensitive to bend.

In these experiments, the step multimode POF is used. The fiber-core diameter and cladding outer diameter are 0.96 and 1.0 mm, respectively. The multi-hole POF is connected to a 650 nm semiconductor laser and a photoelectric converter via couplers. POF is sensitive to heat, but the femtosecond laser micromachining process has virtually no heating effect. The femtosecond laser had a pulse width of approximately 110 fs and a repetition rate of 1 kHz; the laser energy used for the fabrication was approximately 0.5 mJ per pulse. The 800 nm femtosecond laser can process micro-holes and avoid destroying the structure of the optical fiber. The machining results can be seen in Fig. 7. The diameter of each hole is approximately 150 μm.

The impact of the number of holes has on insertion loss while keeping the inter-hole spacing constant is tested. As shown in Fig. 8, the insertion loss grows as the number of holes increases. Next, the impact of inter-hole spacing on insertion loss is tested. As shown

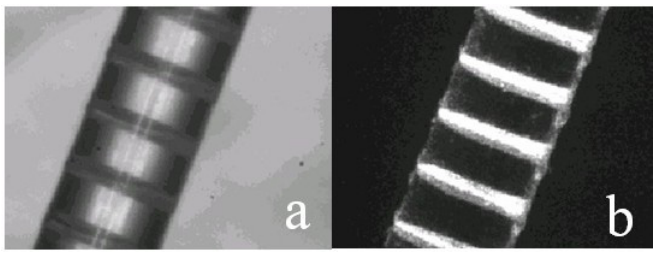

Fig. 7. Side view of multi-hole POF in CCD: (a) not transmitting 650 nm laser and (b) transmitting 650 nm laser.

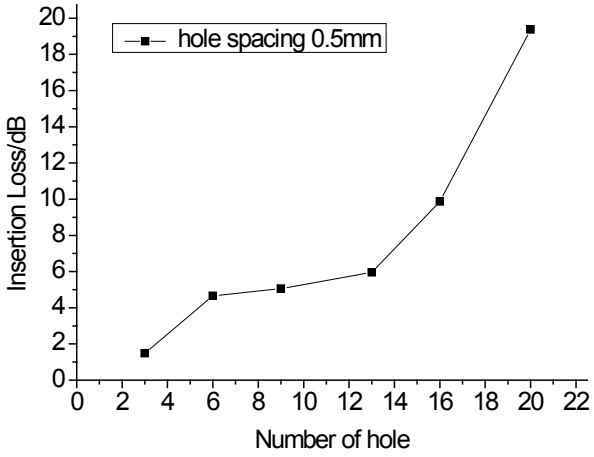

Fig. 8. Relationship between loss and the number of holes with inter-hole spacing set at 0.5 mm.

in Fig. 9, the insertion loss grows at first and then decreases as the inter-hole spacing increases past a certain point. Here, the maximum loss appears when the inter-hole spacing is 1.25 mm. The experimental result is consistent with the theoretical predictions based on the aforementioned loss mechanism.

The schematic diagram of a force sensor is shown in Fig. 10. The sensor mainly comprises spring, cylinder, and force plate. The diameter of the cylinder is 10.0 mm. An annular groove is carved on the periphery. The POF is placed within the groove and the plane of the bend is set perpendicular to the axis of the cylinder. As force is applied against the plate and the spring compresses under the stress, the cylinder will shift downward causing the section of the optical fiber with holes to bend and wind around the cylinder. If the entire said region winds around the cylinder, the sensor's measurement range would reach its maximum. The relationship between force F and loss is studied while the inter-hole spacing is held constant. As shown in Fig. 11, the more

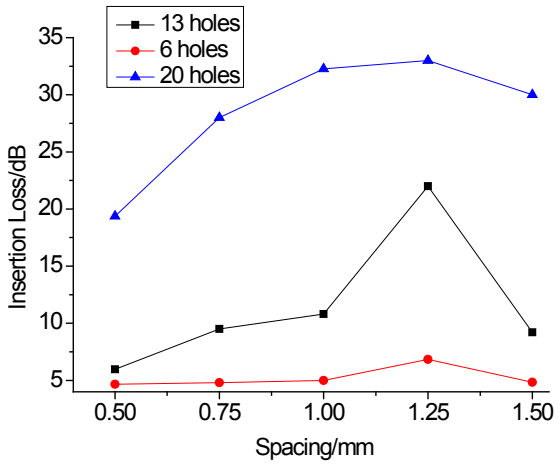

Fig. 9. Relationship between loss and inter-hole spacing with the number of holes at 6, 13, and 20.

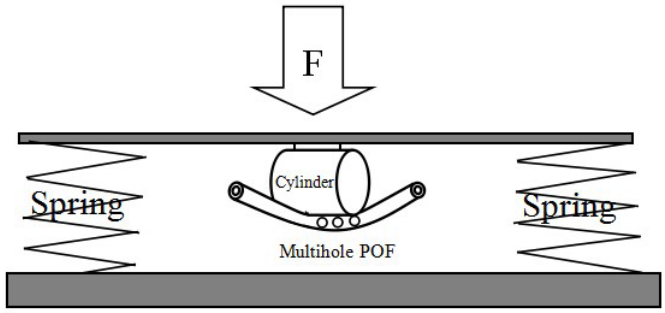

Fig. 10. Schematic diagram of the force sensor.

holes the POF has, the more sensitive the sensor is. The relationship between force F and loss is studied while the inter-hole spacing is varied. As shown in Fig. 9, the insertion loss of a POF with 20 holes is too large, while the measuring range of a POF with 6 holes is too small. Therefore, a POF with 13 holes is the most suitable choice for fabricating the force sensor. For POFs with 13 holes and varied inter-hole spacing, the relationship between loss and force F is shown in Fig. 12. The measurement accuracy increases at first and then decreases as the inter-hole spacing continues to widen. The highest precision occurs when the spacing is set at 1.25 mm; the loss changes over 15.51 dB in the measurable range. At the same time, the insertion loss is also the highest.

Because the POF with spacing of 1.0 mm is sensitive to force and its insertion loss is moderate, it makes a suitable choice for fabricating the force sensor. A sensor fabricated with a POF having 13 holes and spacing of 1.0 mm is tested four times; the result is shown in Fig. 13. Next, we use the structure as shown in Fig. 10 to bend this POF from its initial horizontal position to the extreme and then let it recover to the horizontal

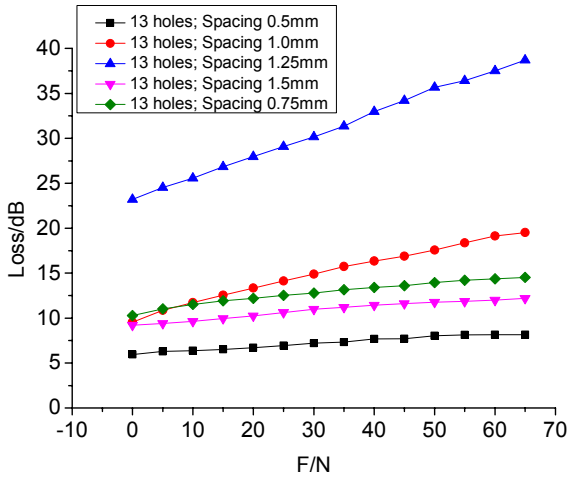

Fig. 12. Relationship between loss and force F for POFs having 13 holes but varied inter-hole spacing.

position; this process is repeated many times. The relationship between the insertion loss at the horizontal position and the number of bend recoveries is shown in Fig. 14. It is thus evident that this particular sensor has the advantages of good repeatability and reliability. The thermal effects on insertion loss of a POF having 13 holes and spacing of 1.0 mm is shown in Fig. 15.

In conclusion, we analyze the effects of hole quantity and inter-hole spacing on insertion loss from both theoretical and experimental aspects. Further, the mechanism of bending loss in multi-hole POF is presented. Bend-sensitive multi-hole POF is made by femtosecond laser micromachining. A force sensor based on bending loss of the multi-hole POF is fabricated. The measurement ranges from 0 to 65 N, and the maximum ranges in output are above 15.51 dB with high linearity and good repeatability, and the sensitivity is 0.24 dB/N.

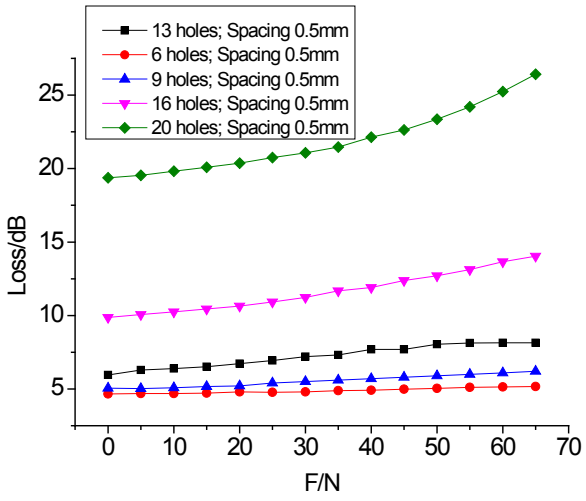

Fig. 11. Relationship between loss and force F for POFs having varied number of holes set 0.5 mm apart.

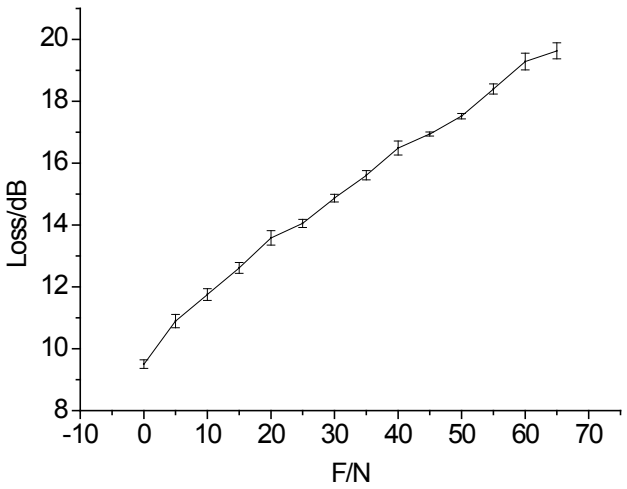

Fig. 13. A sensor fabricated with a POF having 13 holes and spacing of 1.0 mm is tested four times.

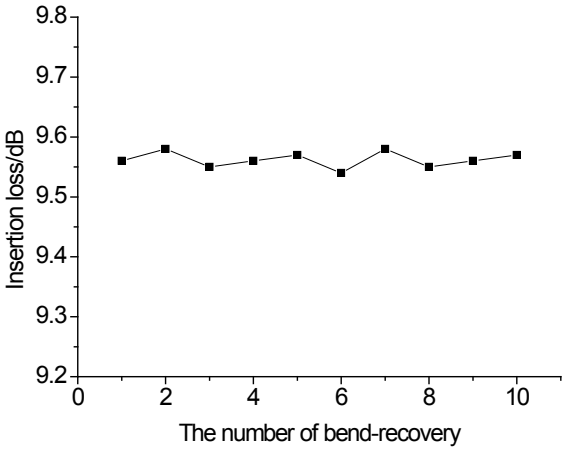

Fig. 14. Relationship between insertion loss at the horizontal position and the number of bend recoveries for a POF having 13 holes and spacing of 1.0 mm.

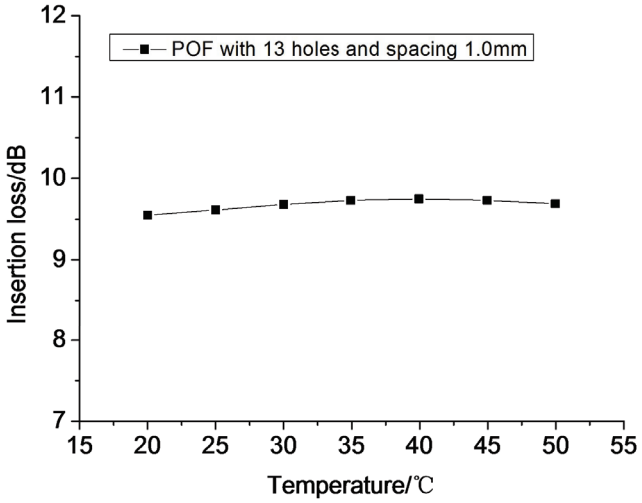

Fig. 15. Thermal effects for insertion loss of POF with 13 holes and spacing of 1.0 mm.

This particular sensor also has the advantages of low cost, simple construction, and quick response.

This work was supported by the National Basic Research Program of China (No. 2011CB921603) and the National Natural Science Foundation of China (No. 11074097).

References

1. Z. Chen, T. T. Teo, S. H. Ng, and X. Yang, in *Proceedings of IEEE Sensors 2012* (2012).
2. M. Morisawa, Y. Amemiya, H. Kohzu, C. X. Liang, and S. Muto, Meas. Sci. Technol. **12,** 877 (2001).
3. A. Babchenko, Z. Weinberger, N. Itzkovich, and J. Maryles, Meas. Sci. Technol. **17,** 1157 (2006).
4. C.-S. Chu and Y.-L. Lo, IEEE Photon. Technol. Lett. **20,** 63 (2008).
5. G. Xin, K. Peng, Z. Gu, J. Zhao, R. Fan, L. Liu, and X. Xu, Chin. Opt. Lett. **11,** 020601 (2013).
6. C. M. Jewart, Q. Wang, J. Canning, D. Grobnic, S. J. Mihailov, and K. P. Chen, Opt. Lett. **35,** 1443 (2010).
7. W. Zhang, L. Liu, F. Li, and Y. Liu, Chin. Opt. Lett. **5,** 507 (2007).
8. L. C. Bobb and H. D. Krumboltz, Opt. Lett. **16,** 112 (1991).
9. W. Ding and Y. Jiang, Opt. Express **20,** 14054 (2012).
10. S. Watson, M. J. Gander, W. N. MacPherson, J. S. Barton, J. D. C. Jones, T. Klotzbuecher, and T. Braune, J. Ott, and F. Schmitz, Appl. Opt. **45,** 5590 (2006).
11. A. Vijayan, S. Gawli, A. Kulkarni, R. N. Karekar, and R. C. Aiyer, Meas. Sci. Technol. **19,** 105302 (2008).
12. J. Hoyo, V. Berdejo, T. T. Fernandez, A. Ferrer, A. Ruiz, J. A. Valles, M. A. Rebolledo, I. Ortega-Feliu, and J. Solis, Laser Phys. Lett. **10,** 105802 (2013).
13. D. Lin, F. He, Y. Liao, J. Lin, C. Liu, J. Song, and Y. Cheng, J Opt. **15,** 025601 (2013).
14. S. Liehr, J. Burgmeier, K. Krebber, and W. Schade, J. Lightwave Technol. **31,** 1418 (2013).
15. Y. Yu, L. Jiang, B. Li, Z. Cao, and S. Wang, Chin. Opt. Lett. **11,** 110603 (2013).
16. Y. Ju, C. Liu, Y. Liao, Y. Liu, L. Zhang, Y. Shen, D. Chen, and Y. Cheng, Chin. Opt. Lett. **11,** 072201 (2013).